

# Finite temperature spectral function of a hole in a quantum antiferromagnet and role of phonons

Satyaki Kar<sup>(1)</sup> and Efstratios Manousakis<sup>(1,2)</sup>

<sup>1</sup>*Department of Physics and MARTECH, Florida State University, Tallahassee, FL 32306-4350, USA and*

<sup>2</sup>*Department of Physics, University of Athens, Penipistimiopolis, Zografos, 157 84 Athens, Greece.*

(Dated: October 26, 2018)

We study thermal broadening of the hole spectral function of the two-dimensional  $t - J$  model (and its extensions) within the non-crossing approximation with and without the contribution of optical phonons. We find that phonons at finite temperature broaden the lowest energy quasiparticle peak, however, the string excitations survive even for relatively strong electron-phonon coupling. Experimental angle resolved photo-emission spectroscopy (ARPES) results compare well with our calculations at finite temperature when we use strong electron-phonon coupling without any adhoc broadening. In addition, we have studied the role of vertex corrections and we find that their contribution allows us achieve the same overall agreement with the ARPES experimental results but using smaller values for the electron-phonon coupling.

PACS numbers: 71.10.-w, 71.10.Fd, 71.27.+a, 74.72.-h, 79.60.-i

## I. INTRODUCTION

The cuprous oxide superconductors show a broad peak near the Fermi energy followed by a “waterfall”-like feature at higher energies in rather recent high resolution angle-resolved-photoemission-spectroscopy (ARPES) measurements<sup>1,2,3</sup>. Calculations based on the  $t - J$  model give a well-defined quasiparticle-like low energy peak and higher energy “string-like” excitations<sup>5,6</sup>. The results obtained from the  $t - J$  and the  $t - t' - t'' - J$  models, using an artificial broadening of the lowest energy peak and of the other peaks corresponding to the string-excitations, agree reasonably well with the experimental spectra<sup>6</sup>. Furthermore, there are similar studies using the Hubbard model and its extensions<sup>8,9,10</sup> also indicating that the above features seen in the ARPES studies could be due to higher energy hole excitations arising naturally in these strongly correlated electronic models.

In this paper we consider the role of finite temperature and of the coupling of the hole to optical phonons, as recent experiments have provided increasing evidence that electron-phonon coupling is strong in cuprates<sup>1,7,11,12</sup>. Our goal is to examine (a) whether or not the string excitations, claimed in Ref. 6 to be the cause of the “waterfall”-like features seen in the ARPES studies, survive the presence of such strongly coupled phonons and (b) whether or not a natural broadening mechanism due to (i) finite-temperature and/or (ii) the coupling to phonons can give a reasonable explanation of the observed features of the ARPES spectra.

Calculations based on the  $t - J$  model at finite temperature have been done using the Lanczos method<sup>17</sup>, quantum Monte Carlo (QMC)<sup>18</sup> and recently using the so-called hybrid dynamical momentum average (HDMA) method<sup>16</sup>. While the results obtained from these methods are quite useful, the conclusions drawn from any one of them should be taken with some caution; for example, the Lanczos method can be applied to very small

size lattices, and the so-called maximum-entropy technique which is utilized by QMC disregards the high energy peaks due to string excitations and other important details of the spectral function. Though the recently used HDMA method takes into account the electron-phonon vertex diagrams and produces the broad lowest energy peak quite well, the values of the coupling constant  $\gamma$  considered is not strong enough to justify the application of the momentum average method<sup>19</sup>.

In this paper we extend the method introduced in Ref. 4 and developed in Ref. 5,6,13, at finite temperature and we also include the role of optical phonons. In Refs. 4,5 the boson degrees of freedom were treated within the so-called spin-wave approximation and their coupling to electron and hole degrees of freedom is linearized with respect to boson creation operators. Furthermore, the self-consistent Dyson’s equation for the single-hole spectral function was solved within the so-called non-crossing approximation (NCA) where only topologically “planar” diagrams are retained. In the present paper we work within the same linearized Hamiltonian and we include the linear coupling to optical phonons as captured by the Holstein electron-phonon interaction. The calculations are carried out at finite temperature by solving the Dyson’s equation within the NCA for both diagrams which include propagation of spin-wave excitations and diagrams which include phonon propagation. We find that together the phonons with the inclusion of the thermal broadening at room temperature give rise to a broadened spectral function which exhibits similar characteristics to those found in the ARPES studies. More precisely, the conclusions of Ref. 6 are valid without the need to artificially broaden the spectral function. Furthermore, as it is well-known the leading vertex correction due to coupling to spin-waves is zero and other higher order vertex corrections give negligible contribution<sup>13</sup>. In the present calculation we include the leading (two-loop) vertex corrections due to the hole-phonon coupling and due to the coupling of the hole to

spin-wave excitations and we conclude that their contribution allows us achieve the same qualitative agreement with the experimentally determined hole spectral function using smaller values of the electron-phonon coupling constant.

In the following section (Sec. II) we describe the formalism and the approach. In Sec. III we present our results for the spectral function obtained by a numerical solution of the Dyson's equation. In Sec. IV we compare our results with the experimentally determined spectral function. In Sec. V we include the contribution of the vertex corrections and in Sec. VI we present the main conclusions drawn from the present study.

## II. FORMULATION

The motion of a single hole in a spin- $\frac{1}{2}$  Heisenberg antiferromagnet<sup>14</sup> in a two-dimensional(2D) square lattice has been extensively studied using the two-dimensional (2D)  $t - J$  model<sup>6</sup>:

$$H = -t \sum_{\langle i,j \rangle, \sigma} (c_{i\sigma}^\dagger c_{j\sigma} + h.c.) + \sum_{\langle i,j \rangle} [JS_i^z S_j^z + \frac{J_{xy}}{2}(S_i^+ S_j^- + S_i^- S_j^+)]. \quad (1)$$

The first term is the usual hole-hopping term which operates in a space of singly occupied sites and the second and third form the usual Hamiltonian of the Heisenberg antiferromagnet where we have allowed for a possible anisotropy of the coupling between the  $z$  and the perpendicular spin components. While this Hamiltonian has been thoroughly studied during the last almost two decades using many techniques, only a handful of methods are shown to yield accurate results in certain limits. For the case of a single hole spectral function, one of such rather successful techniques is the so-called self-consistent Born approximation (SCBA)<sup>5</sup>.

A simple way to introduce the coupling of the hole motion to a single optical phonon branch is by adding to the  $t - J$  model an electron-phonon coupling term by means of the following Holstein term:

$$H_{el-ph} = \Omega_0 \sum_k b_k^\dagger b_k + \frac{\gamma}{\sqrt{N}} \sum_{k,q} c_k^\dagger c_{k-q} b_q + h.c. \quad (2)$$

where  $b^\dagger$  is the optical-phonon creation operator,  $\Omega_0$  is a characteristic optical phonon frequency and  $\gamma$  is the electron-phonon coupling constant.

Within the linear spin-wave approximation, using the Bogoliubov transformation to diagonalize the Heisenberg term and and by linearizing the hopping term with respect to the spin-deviation operators, one finds<sup>4,5</sup> the following expression for the Hamiltonian given by Eq. 1:

$$H = E_0 + J \sum_{\mathbf{k}} (f_{\mathbf{k}}^\dagger f_{\mathbf{k}} + h_{\mathbf{k}}^\dagger h_{\mathbf{k}}) + \sum_{\mathbf{k}} \omega_{\mathbf{k}} (\alpha_{\mathbf{k}}^\dagger \alpha_{\mathbf{k}} + \beta_{\mathbf{k}}^\dagger \beta_{\mathbf{k}})$$

$$+ \sum_{k,q} h_k^\dagger f_{k-q} [g(k,q)\alpha_q + g(k-q,-q)\beta_{-q}^\dagger] + f_k^\dagger h_{k-q} [g(k-q,-q)\alpha_{-q}^\dagger + g(k,q)\beta_q] + H.c. \quad (3)$$

The function  $g(k,q)$  which plays the role of the hole-spin wave coupling constant is defined in Refs. 4,5.

In order to calculate the effects of finite temperature we will use the Matsubara technique followed by analytic continuation to the real frequencies to obtain the reduced Green's function<sup>20,21</sup>. The self-consistent solution to Dyson's equation for the self energy of the Hamiltonian given by Eq. 3 is obtained by iterating the following equation with respect to  $n$ :

$$\begin{aligned} \Sigma_{(n+1)}(\mathbf{k}, \omega) &= \sum_{\mathbf{q}} g^2(\mathbf{k}, \mathbf{q}) \left[ N_{\mathbf{q}} G_n(\mathbf{k} - \mathbf{q}, \omega + \omega_{\mathbf{q}}) + \right. \\ &\quad \left. (1 + N_{\mathbf{q}}) G_n(\mathbf{k} - \mathbf{q}, \omega - \omega_{\mathbf{q}}) + \int_{-\infty}^{\infty} \frac{d\epsilon}{\pi} n_F(\epsilon) D_0(\mathbf{q}, \epsilon - \omega) \text{Im} G_r(\mathbf{k} - \mathbf{q}, \epsilon) \right] \\ G_n(\mathbf{k}, \omega) &= \frac{1}{\omega - \xi_{\mathbf{k}} - \Sigma_n(\mathbf{k}, \omega)} \end{aligned} \quad (5)$$

where  $N_{\mathbf{q}} = n_B(\omega_{\mathbf{q}})$ , with  $n_B(\omega) = \frac{1}{e^{\beta\omega} - 1}$ , and  $n_F(\xi_{\mathbf{q}}) = \frac{1}{e^{\beta\xi_{\mathbf{q}}} + 1}$ . Also,  $\xi_{\mathbf{k}} = \epsilon_{\mathbf{k}} - \mu$ , where  $\epsilon_{\mathbf{k}}$  is the zeroth order hole energy, which according to Eq. 3 is equal to  $J$ , and  $\mu$  is the chemical potential. Here  $\omega_{\mathbf{q}}$  is the spin-wave frequency,  $D_0$  is the spin-wave propagator given as follows:

$$D_0(\mathbf{q}, \omega) = \frac{2\omega_{\mathbf{q}}}{\omega^2 - \omega_{\mathbf{q}}^2}. \quad (6)$$

and  $G_r(\omega, k)$  is the retarded Green's function which is obtained from the Matsubara Green's function by analytic continuation:

$$G_r(\mathbf{k}, \omega) = \lim_{\delta \rightarrow 0} G(\omega + i\delta, k). \quad (7)$$

In the case where we include the coupling to the optical phonons via Eq. 2 we need to add to the above expression for the self-energy three more terms which are the same as the above and they are obtained from the above expressions by replacing the hole-spin-wave coupling constant  $g$  by  $\gamma/\sqrt{N}$ , and the spin-wave frequency by the phonon frequency  $\Omega_0$ .

While the first two terms of the above equation are of order unity, it can be shown that the last term is of order of  $1/N$  because we only consider a single hole. This can be seen by considering the following identity

$$N_h = \sum_p \int_{-\infty}^{\infty} n_F(\omega) A(p, \omega). \quad (8)$$

The difference between this equation and the third term of Eq. 4 is the presence of boson propagator,  $D_0$  which is not an extensive quantity. Hence, the order of magnitude of the last term in Eq. 4 is  $\sim O(N_h/N)$  and vanishes in the thermodynamic limit.

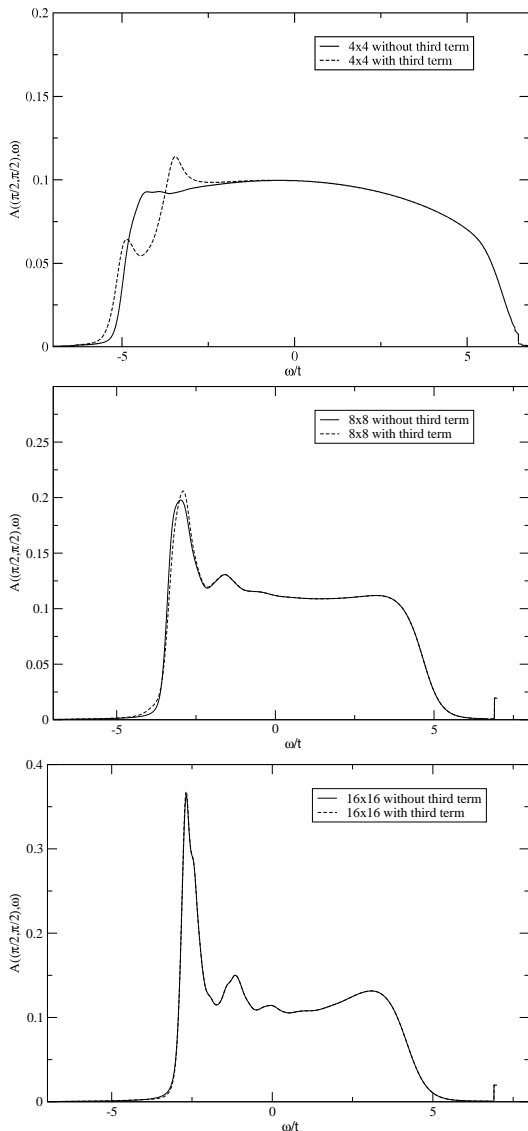


FIG. 1: The calculated spectral function for  $\mathbf{k} = (\frac{\pi}{2}, \frac{\pi}{2})$  for  $\beta t = 10$  for a  $4 \times 4$  (top),  $8 \times 8$  (middle) and  $16 \times 16$  (bottom) lattice with (dashed line) and without (solid line) the inclusion of the third term in the self-energy expression given by Eq. (4)

The vanishing of the third term in Eq. 4 is also demonstrated numerically in Fig. 1 which shows the spectral function for  $(\frac{\pi}{2}, \frac{\pi}{2})$  with and without the third term in Eq. 4 for  $\beta t = 10$  and for  $4 \times 4$ ,  $8 \times 8$  and  $16 \times 16$  lattices respectively. The solid lines are the spectral functions without the third term while the dashed lines are obtained by including it by means of a single iteration of Eqs. 4,5. Notice that for large enough size lattice the contribution of this term becomes negligible. In the rest of our calculations presented in this paper this term will be neglected.

The self-consistent Dyson's equation in conjunction with the so-called non-crossing approximation (NCA) (crossing diagrams have a small contribution as explained in Refs. 5,13) is solved by means of an iterative procedure

to obtain the dressed hole propagator and the hole spectral function. For numerical calculations a small converging parameter  $\eta$  is needed in the zeroth order Green's function as follows

$$G^{(0)}(k, \omega) = \frac{1}{\omega - \xi_k + i\eta}. \quad (9)$$

Starting from the above zeroth order approximation for the single hole Green's function, the Dyson's equation is iterated until convergence is achieved. Because the lowest-energy quasiparticle peak corresponds to a well-defined excitation, its width and height, as smaller and smaller values of  $\eta$  are used, scale proportionally to  $\eta$  and  $1/\eta$  respectively. In addition, in order to avoid finite-size effects a smaller value of  $\eta$  requires a larger size lattice. In Ref. 5 it was demonstrated that the single hole spectral function has negligible finite-size effects for lattices larger than  $16 \times 16$  when a value for  $\eta = 0.1t$  was used. However, when we take smaller values of  $\eta$ , we need bigger size lattices to eliminate the finite-size effects. For example, at  $T = 0$  and without phonons, we have found that in order to reach the thermodynamic limit for  $\eta/t = 0.1$ , a  $16 \times 16$  size-lattice is large enough, while if we take  $\eta/t = 0.05$  or  $\eta/t = 0.01$  lattices of sizes  $24 \times 24$  and  $32 \times 32$  respectively are required.

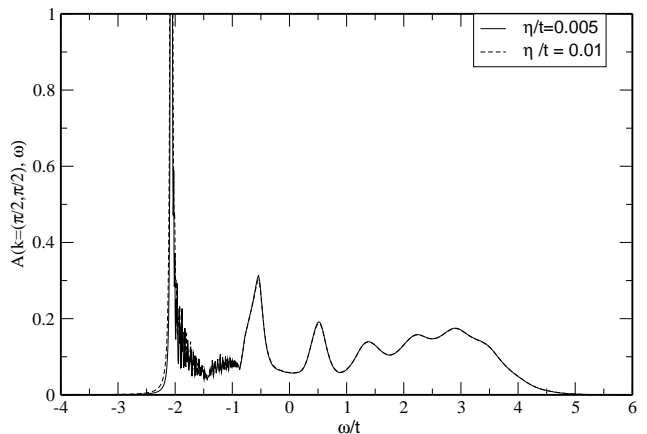


FIG. 2: The single-hole spectral function at  $T = 0$  with  $\gamma = 0$  for  $(\frac{\pi}{2}, \frac{\pi}{2})$  calculated on a  $64 \times 64$  lattice with  $\eta = 0.005t$  (solid line) and  $0.01t$  (dashed line).

Since the quasiparticle peak is a well-defined excitation<sup>5</sup> at  $T = 0$ , its height becomes greater as we decrease  $\eta$ . On the other hand in the higher energy part of the spectral function, because it forms a continuum of states, the various Lorentzian contributions overlap strongly because the energy spacing  $\Delta\epsilon$  of neighboring energy levels becomes exponentially small with lattice size, i.e.,  $\Delta\epsilon \sim e^{-\alpha N}$  (where  $N = L \times L$  is the number of lattice sites). Fig.2 shows the  $(\frac{\pi}{2}, \frac{\pi}{2})$  spectral function with  $\eta = 0.01t$  and  $0.005t$  for a  $64 \times 64$  size lattice.

The difference is mainly in the height of the lowest energy peak which doubles by decreasing the value of  $\eta/t$  by a factor of 2 and the other parts of both of the spectral functions are very close. In this paper we have used  $J = 0.3t$  and  $\eta = 0.05t$ .

### III. NUMERICAL RESULTS

#### A. Finite temperature no phonons

First of all we study the effect of temperature alone, i.e., without any phonons in the system. Fig. 3 shows the spectral function for  $\mathbf{k} = (\frac{\pi}{2}, \frac{\pi}{2})$  for  $T/t = 0.001, 0.01, 0.05, 0.1$  and  $0.15$ , calculated on a  $16 \times 16$  lattice. As the thermal broadening is most prominent near the lowest energy well-defined peak, notice that the multi-peak structure of the spectral function just above the lowest peak becomes more and more broadened as the temperature is raised. The effect of finite temperature is also to move the low energy peaks towards lower energies (a shift of about  $0.05t$  occurs for  $T = 0.1t$ ). In Fig. 4, we present the spectral function for  $\mathbf{k} = (0,0)$  using the same values of  $\beta$ . Notice that the peaks which correspond to string excitations are robust even for temperature as high as  $T = 0.15t$  for both cases of the spectral functions.

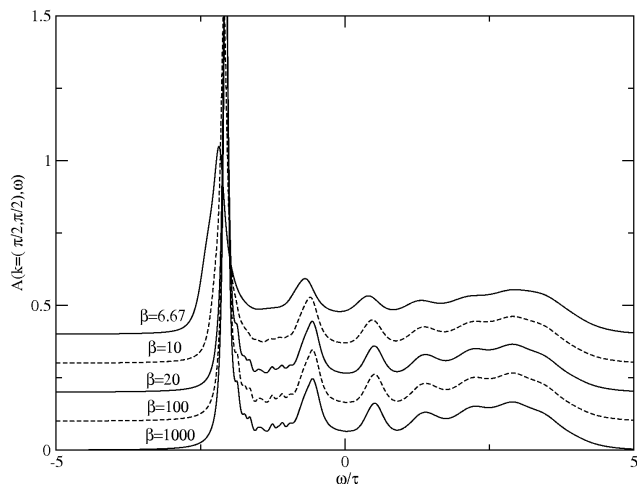


FIG. 3: Hole spectral function for  $(\frac{\pi}{2}, \frac{\pi}{2})$  without phonons for a  $16 \times 16$  lattice and for  $\beta t = 1000, 100, 20, 10$ , and  $6.67$ .

An intensity plot for  $\beta t = 10$  is presented in Fig. 5 along with the ARPES intensity<sup>2</sup>. Notice that there is a significant gap or pseudo-gap between the lowest energy peak and the first string excitation and also between the first string excitation and the peak which evolves to become an intense peak near  $(0,0)$ . In the following we will discuss that the presence of optical phonons which couple strongly to the hole excitations can remove these gaps

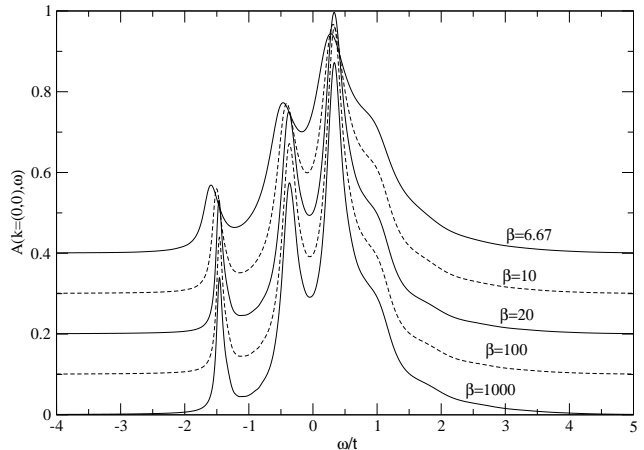


FIG. 4: Spectral function for  $\mathbf{k} = (0,0)$  without phonons for a  $16 \times 16$  lattice using  $\beta t = 1000, 100, 20, 10$  and  $6.67$ .

and make the intensity graph similar to those observed in ARPES.

#### B. Optical Phonons at $T = 0$

As it has been demonstrated the NCA is a good approximation for the case of the single-hole in the pure  $t - J$  model, we need to make sure that it also works for the case of the perturbative expansion involving terms in which the boson loops are due to the phonon propagator. Mishchenko et al.<sup>15</sup> have shown that by increasing the value of the electron-phonon coupling strength  $\gamma$  and at zero temperature, a cross-over between the lowest state and the next string state takes place at  $\gamma \sim 0.4t$  and from there on the lowest state which is like a narrow quasiparticle peak always stays dispersionless. According to their calculation the next high energy state shows broadening just as it also appears in the experimental ARPES plot<sup>2</sup>. Surprisingly the results of Mishchenko et al.<sup>15</sup> with no phonons do not completely agree with earlier numerical results<sup>5</sup>. Here, we will study the effect of non-crossing diagrams at finite temperature using this  $t - J$ -Holstein model with  $\gamma$  both below and above the cross-over point<sup>15</sup> and then compare our results with experimentally obtained intensity plots.

Experimental values of characteristic phonon energy scales vary from  $30 - 80 meV$ <sup>1,15</sup>. It is rather well known that the value of  $t$  is approximately  $0.4eV$  for the cuprate materials and we have used  $\Omega_0 \sim 0.1t$  and  $0.2t$  both producing essentially the same spectral functions<sup>15</sup>.

In Fig. 6 the spectral function for  $\mathbf{k} = (\frac{\pi}{2}, \frac{\pi}{2})$  and for  $\Omega_0 = 0.1t$  with  $\gamma = 0.0, 0.1, 0.2, 0.4, 0.5$  and  $1.0$  calculated on a  $16 \times 16$  size lattice is presented. These results demonstrate that the string excitations are quite robust in the presence of optical phonons. In addition, in Fig. 7

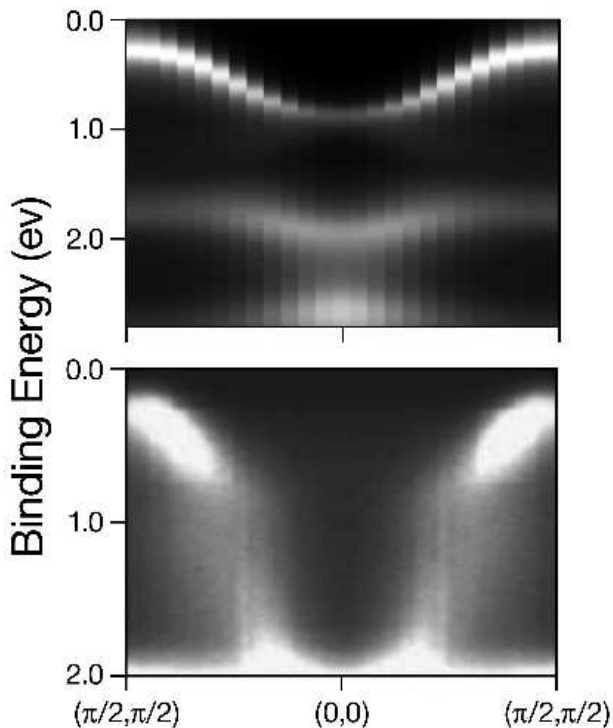


FIG. 5: Top: Calculated intensity plot on a  $48 \times 48$  lattice at  $\beta t = 10$  and no phonons. Bottom: ARPES intensity along the  $(0,0)$  to  $(\pi/2, \pi/2)$  direction.

the  $\mathbf{k} = (0,0)$  spectral function is shown, for  $\Omega_0 = 0.1t$  with  $\gamma = 0.0, 0.1, 0.2, 0.4, 0.5$  and  $1.0$  as calculated on a  $16 \times 16$  size lattice. The same conclusion about the robust nature of the string excitations can also be drawn from this graph.

The spectral function calculated for  $J = 0.3t$  has some saw-teeth-like features at energy just above the lowest peak. Particularly we can see that the 1st such peak closest to the lowest energy quasiparticle peak ( $\sim 0.2t$  energy apart) gains weight as the value of  $\gamma$  is increased more and more, a feature which is also observed in DMC<sup>15,16</sup> and in the HDMA<sup>16</sup> calculations at zero temperature. By increasing the value of  $\gamma$  the low energy peaks move towards lower energies. For values of  $\gamma$  of about  $0.5t$  this energy shift becomes approximately  $0.1t$ . When  $\gamma = 1.0t$ , however, this energy shift becomes large ( $\sim 0.4t$ ). However, NCA is not expected to be a good approximation to describe the spectral function for  $\gamma = 1.0t$ . Also NCA does not show the cross-over phenomena as referenced by Mishchenko et al.<sup>15</sup>.

Phonons cannot broaden the lowest peak at zero temperature (due to energy conservation requirement) though the higher energy peaks corresponding to string states are broadened more and more with  $\gamma$ . In the next subsection (and Fig. 8) we discuss that thermal broad-

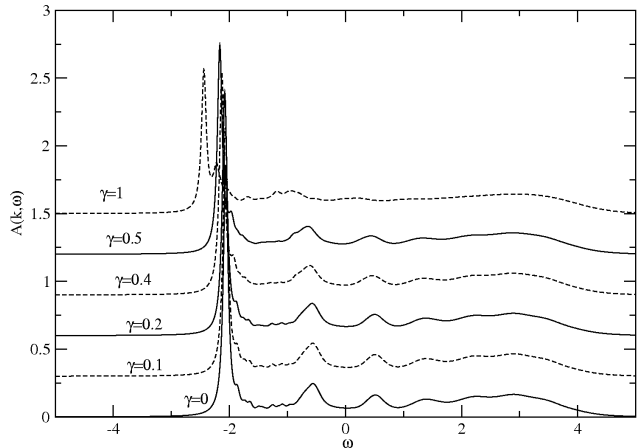


FIG. 6: Zero-temperature spectral function at  $\mathbf{k} = (\frac{\pi}{2}, \frac{\pi}{2})$  on a  $16 \times 16$  size lattice with optical phonons and  $\Omega_0 = 0.1t$  and for  $\gamma$  ranging from 0 to 1.0.

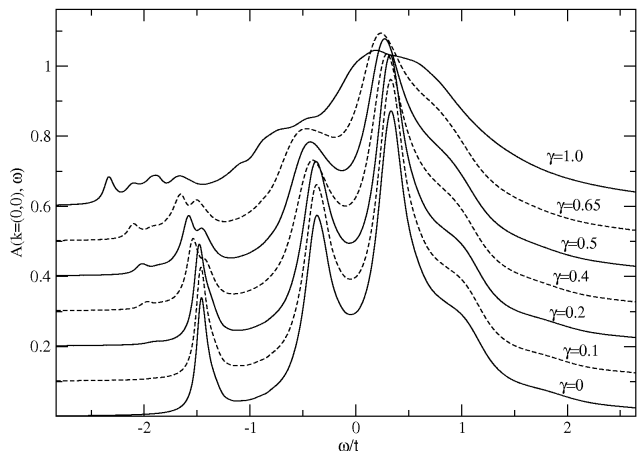


FIG. 7: Calculated spectral function for  $\mathbf{k} = (0,0)$  and at zero temperature for a  $16 \times 16$  size-lattice for  $\gamma = 0.0, 0.1, 0.2, 0.4, 0.5, 0.65$  and  $1.0t$ .

ening plays an important role in filling up the gap between the lowest peak and the next phonon-generated small peak making an overall broad lowest energy peak.

### C. Finite temperature and optical phonons

Fig. 8 shows the vicinity of the lowest energy peak of the calculated spectral function for  $\mathbf{k} = (\frac{\pi}{2}, \frac{\pi}{2})$  for  $\beta = 1000, 100, 20, 10$  and  $6.67$ , and with  $\Omega_0 = 0.1t$  and  $\gamma = 0.5t$  (Fig. 8.a) and  $\gamma = 1.0t$  (Fig. 8.b) on a  $16 \times 16$  lattice. Notice that for both cases of electron-phonon

coupling, as the temperature rises the lowest peak and the next phonon-induced peak smears due to thermal broadening and this gives rise to a single broad peak as seen in Fig. 8. This is the mechanism by means of which the lowest energy peak acquires a width of the same size as that found experimentally. A width of similar magnitude was used in Ref. 6 to obtain agreement with the ARPES intensity.

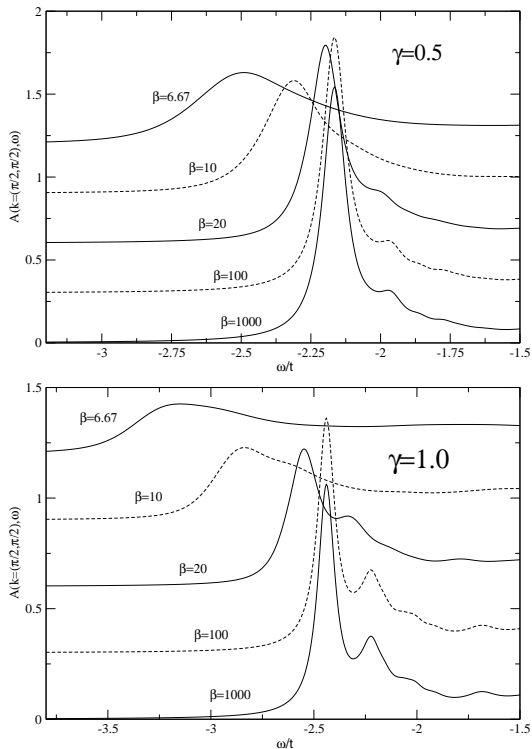


FIG. 8: The spectral function for  $\mathbf{k} = (\frac{\pi}{2}, \frac{\pi}{2})$  calculated on a  $16 \times 16$  size lattice for  $\beta t = 1000, 100, 20, 10$  and  $6.67$  at  $\gamma = 0.5t$ (top) and  $\gamma = 1.0t$ (bottom). Only the vicinity of the lowest energy peak is shown.

The effects of the electron-phonon interaction are presented in Fig. 9, in a much wider frequency range, for  $\mathbf{k} = (\frac{\pi}{2}, \frac{\pi}{2})$  and for  $\beta t = 10$  and for  $\gamma/t = 0, 0.1, 0.2, 0.4, 0.5$  and  $1.0$ , where  $\Omega_0 = 0.1t$  was used in this calculation. In Fig. 10 the spectral function for  $k = 0$  and electron-phonon coupling  $\gamma = 0.5t$  and for various values of temperature is shown.

In Fig. 11(top) we present the calculated dispersion of the lowest energy quasiparticle peak for the  $t-J$ -Holstein model for various values of the electron-phonon coupling in the range  $\gamma/t = 0 - 1$ . In Fig. 11(bottom) we present the same calculation carried out for the  $t-t'-t''-J$  model for the parameter values believed to be needed in order to reproduce the ARPES data<sup>6,12</sup>. Notice that the only significant effect on the  $t-t'-t''-J$  model, is to shift the overall energy by a constant and does not alter

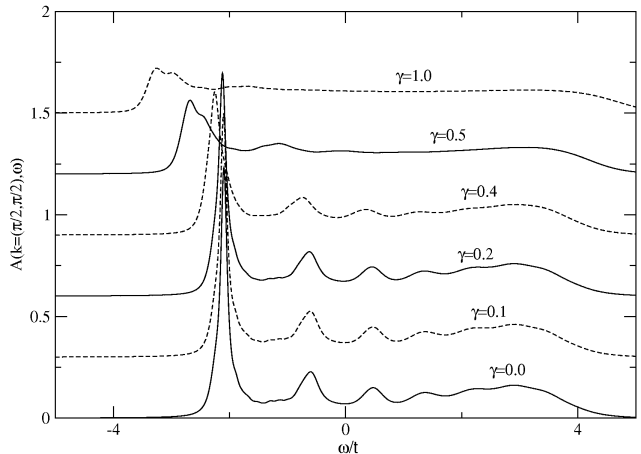


FIG. 9: The spectral function for  $\mathbf{k} = (\frac{\pi}{2}, \frac{\pi}{2})$  for  $\beta = 10t$  on a  $16 \times 16$  size lattice for  $\gamma = 0.0, 0.1, 0.2, 0.4, 0.5$ , and  $1.0$ .

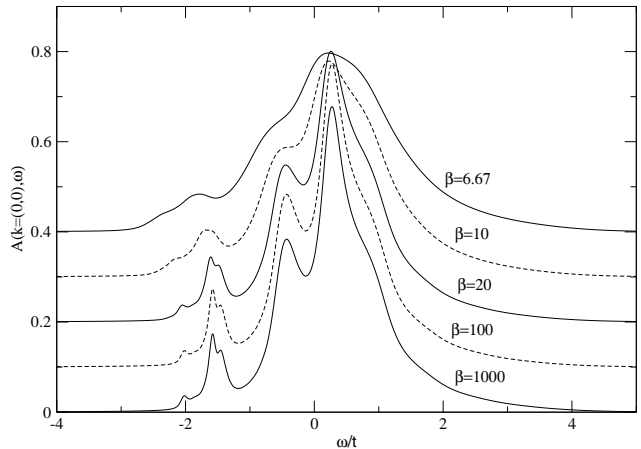


FIG. 10: The spectral function for  $k = (0, 0)$  for  $\gamma = 0.5t$  calculated on a  $16 \times 16$  size lattice and for  $\beta t = 1000, 100, 20, 10$  and  $6.67$ .

the features of the dispersion. The effect of phonons on the hole dispersion for the case of the pure  $t-J$  model is more significant(Fig. 11).

#### IV. COMPARISON WITH ARPES

The observed ARPES spectral function reveals that the lowest energy peak for  $\mathbf{k} = (\frac{\pi}{2}, \frac{\pi}{2})$  has a width  $\sim 0.4eV$  and it is the most intense feature together with the one near  $\mathbf{k} = (0, 0)$ . As we move from  $(\frac{\pi}{2}, \frac{\pi}{2})$  towards  $(0, 0)$ , the lowest energy peak moves gradually towards higher energies and a second peak grows near  $\mathbf{k} = (0, 0)$ . At around  $\mathbf{k} = (\frac{\pi}{4}, \frac{\pi}{4})$  the intensity of the lowest energy

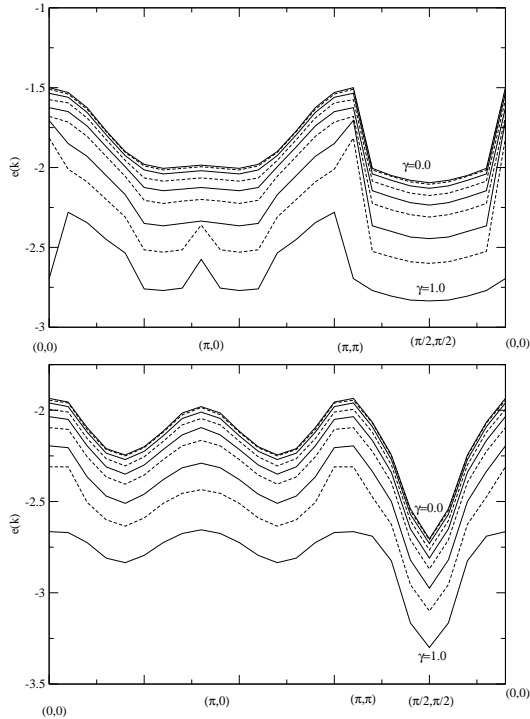


FIG. 11: The hole band for  $\beta t = 10$  and for various values of  $\gamma$  for (top) the  $t - J$  model and (bottom) the  $t - t' - t'' - J$  model with  $t' = -0.33t$ ,  $t'' = 0.22t$ . The values  $\gamma/t = 0.0, 0.1, 0.2, 0.3, 0.4, 0.5, 0.65, 0.8$  and  $1.0$  were used in both graphs

peak decreases appreciably and also smears over a region of higher energy. It is possible to explain these observations using the results of the calculation based on the  $t - J$  model and the NCA as reported in Ref. 6 where the contribution of the string excitations gives rise to rather well-defined peaks in the spectral function at higher energy, provided that these string excitation peaks broaden significantly at around  $(\frac{\pi}{4}, \frac{\pi}{4})$  to give rise to some rather flat-intensity region. Furthermore, near  $\mathbf{k} = (0, 0)$ , the peak which corresponds to a higher energy string excitation suddenly picks up intensity while the broadening process of the other string excitation peaks still prevails. This combined process of spectral-weight transfer and broadening of the peaks gives rise to the observed energy kinks in the ARPES intensity. However, these have been reported to be due to the electron-phonon interactions<sup>11,22</sup> and the two energy scales separating the intermediate smeared intensity region from the two peaks on the two sides (one at  $(\frac{\pi}{2}, \frac{\pi}{2})$  and the other at  $(0, 0)$ ) has been identified as the threshold of disintegration of the low-energy quasi-particles into a spinon and a holon branch<sup>3</sup>.

The role of temperature is to broaden the high energy string excitation peaks though the effect is not very pronounced<sup>12</sup> without simultaneously introducing the electron-phonon coupling. Fig. 12 shows the spectral

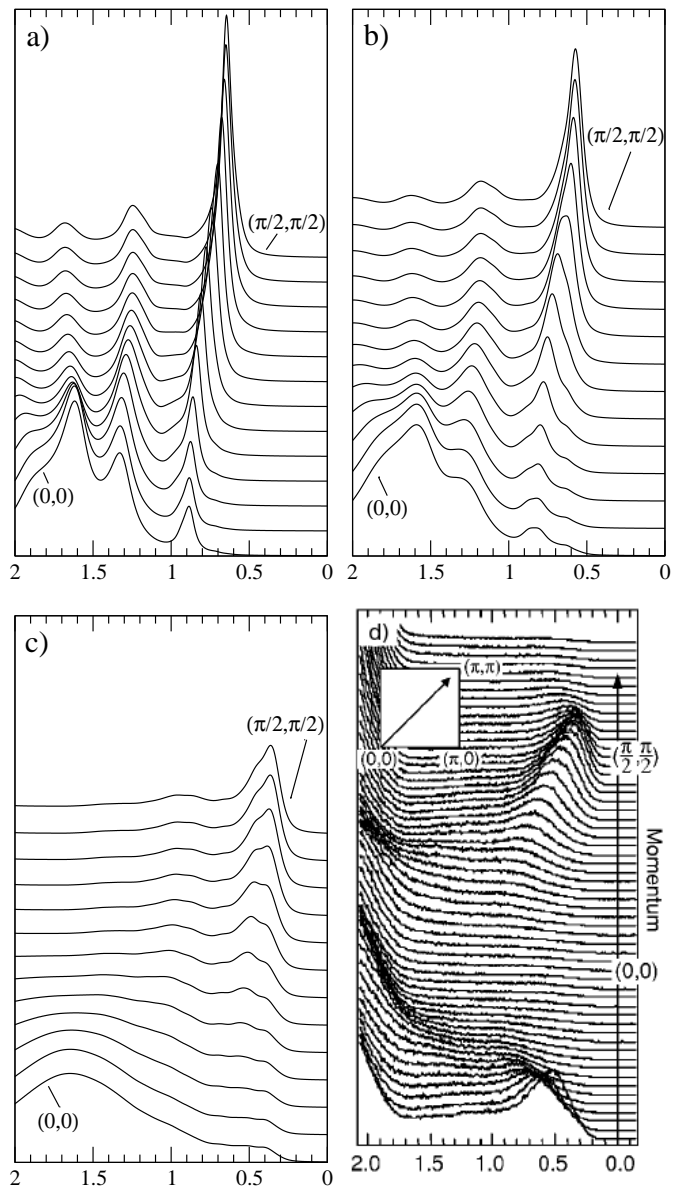


FIG. 12: The top-left, top-right and bottom-left spectral functions are along  $(0,0) \rightarrow (\frac{\pi}{2}, \frac{\pi}{2})$  and they are calculated for electron-phonon coupling  $\gamma/t = 0.2, 0.5$  and  $1.0$  respectively on  $48 \times 48$  lattice. The bottom-right spectral function is the one obtained experimentally in ARPES.

function for all values of  $\mathbf{k}$  along the  $(0, 0) \rightarrow (\frac{\pi}{2}, \frac{\pi}{2})$  direction on a  $48 \times 48$  lattice for  $\beta = 10$ ,  $\Omega_0 = 0.1t$  and for electron-phonon coupling  $\gamma/t = 0.2, 0.5$ , and  $1.0$  and it is compared with experimentally obtained ARPES spectral function<sup>2</sup>. For  $\mathbf{k}$  around  $(\frac{\pi}{4}, \frac{\pi}{4})$ , where the height of the lowest peak and the higher energy string excitations are almost equal, the combined effect of the electron-phonon coupling and the finite temperature produces flat regions with much less intensity (than that of the lowest peak) in the spectral functions. Notice that using  $\gamma = 0.2$  and  $0.5t$ , which are below and near the possible cross-over point<sup>15</sup>, the high energy peak structure due to string ex-

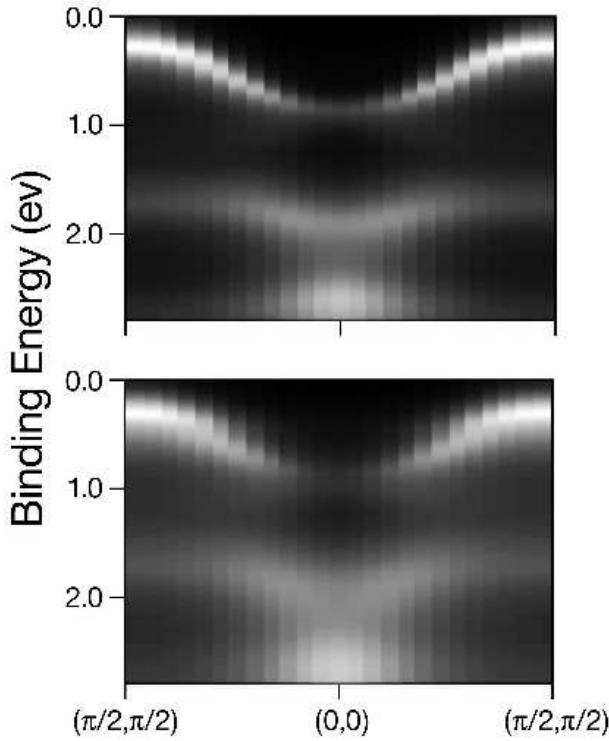


FIG. 13: Intensity plot of a  $48 \times 48$  lattice at  $\beta = 10$  for  $\gamma = 0.2$  (top) and  $0.5$  (bottom)

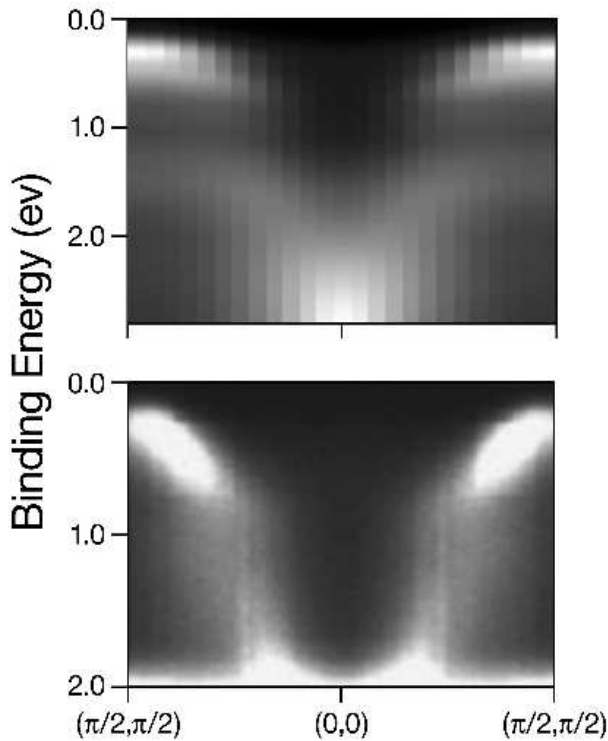


FIG. 14: The theoretical intensity plot for a  $48 \times 48$  lattice at  $\beta = 10$  and for  $\gamma = 1.0$  (top) is compared with the experimentally obtained ARPES spectra (bottom).

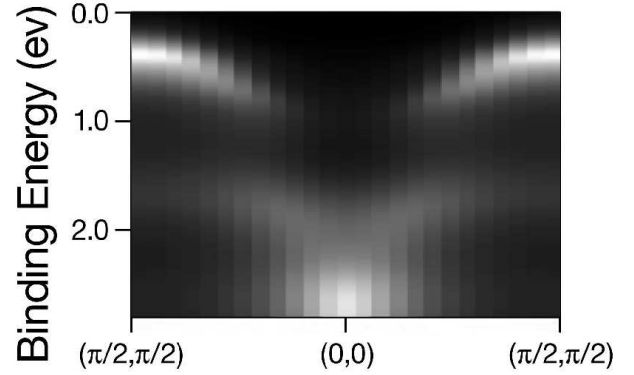


FIG. 15: Intensity plot calculated on a  $48 \times 48$  lattice for  $\gamma = 0.5t$  and  $\beta t = 6.67$

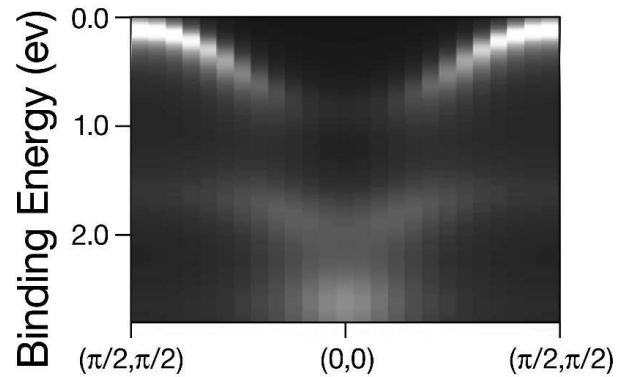


FIG. 16: Intensity plot calculated on a  $48 \times 48$  lattice at  $\gamma = 0.5t$  and for  $\beta t = 10$  with  $t' = -0.33t$ ,  $t'' = 0.22t$

citations becomes visible at around  $\mathbf{k} = (\frac{\pi}{4}, \frac{\pi}{4})$  and it is broadened. This mechanism creates a flat, low intensity region which becomes more pronounced for  $\gamma = 1.0t$ . We note that in order for our NCA based calculation without vertex corrections to produce spectral functions and intensity plot (Fig. 14) similar to that obtained by ARPES we need to increase the value of  $\gamma/t$  to  $1.0$  (for  $\beta t = 10$ , which corresponds approximately to room-temperature). It also can be observed that as we move from  $(\frac{\pi}{2}, \frac{\pi}{2})$  to  $(0, 0)$  the peak structure which corresponds to string excitations becomes compressed more and more as a function of energy and the peaks are closest to each other at  $(0, 0)$ .

The same features can also be seen in Figs. 13,14 which present the intensity plot on a  $48 \times 48$  lattice (for  $\beta = 10$ ,  $\Omega_0 = 0.1t$ ) and for the same three values of  $\gamma/t = 0.2$  (top part of Fig. 13),  $0.5$  (bottom part of Fig. 13), and  $1.0$  (top part of Fig. 14) and it is compared with experimentally obtained ARPES spectral functions (bottom part of Fig. 14). Notice that the intensity plot becomes comparable to the experimentally obtained ARPES spectral function when we use a large value of the electron-phonon  $\gamma$ . As discussed in the following section, the presence of vertex corrections due to electron-phonon-coupling al-



lows us to use a smaller value of  $\gamma$  to achieve the same qualitative agreement with the ARPES intensity.

Since the value of  $t$  is not accurately known, we do not have a precise knowledge of the value of room temperature in units of  $t$ . Hence, we also tried higher temperature,  $T = 0.15t$ , where more broadening is obtained. As can be noticed from Fig. 15, where  $\gamma/t = 0.5$  was used, temperature could be an additional factor which helps us achieve better agreement with the observed intensity plot without having to increase the value of  $\gamma$  and enter a domain where the validity of NCA becomes questionable.

As we are mainly interested for intensity plots along the  $(0, 0)$  to  $(\pi/2, \pi/2)$  cut in the  $\mathbf{k}$ -space, the inclusion of  $t'$  and  $t''$  also does not change the spectral functions very much, as can be seen in Fig. 16, where the  $t - t' - t'' - J$  model was used, taking  $t' = -0.33t$  and  $t'' = 0.22t$  and in addition  $\beta = 10$  and  $\gamma = 0.5t$ .

## V. VERTEX CORRECTIONS

The electron-phonon vertex corrections are expected to be important for the hole-spectra unlike the electron-spin-wave vertex corrections whose contribution have been found to be small<sup>13</sup>. There are some recent cal-

culations indicating the discrepancy between the spectral function with and without vertex correction in the strong phonon coupling regime at zero temperature<sup>15?</sup>. In this section, we present the results of our study of the role of such vertex corrections, namely we improve the NCA by including the leading-order vertex corrections due to the electron-phonon coupling. The contributions to the

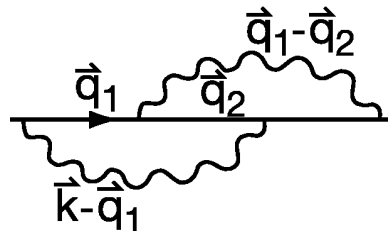


FIG. 17: The leading vertex correction to the hole Green's function due to its coupling to phonons.

self-energy are shown in the diagrams of Figs. 17,18 and following the procedure outlined in Ref. 20 we obtain the following expressions:

$$\begin{aligned} \Sigma^{(\alpha)}(\omega, \mathbf{k}) = & \sum_{\sigma=\pm 1} \sum_{\mathbf{q}_1, \mathbf{q}_2} G(\omega - \sigma\omega_{\mathbf{k}-\mathbf{q}_1}^{(p)}, \mathbf{q}_1) \left[ N_{\mathbf{q}_1-\mathbf{q}_2}^{(\alpha)} G(\omega - \sigma\omega_{\mathbf{k}-\mathbf{q}_1}^{(p)} + \omega_{\mathbf{q}_1-\mathbf{q}_2}^{(\alpha)}, \mathbf{q}_2) G(\omega + \omega_{\mathbf{q}_1-\mathbf{q}_2}^{(\alpha)}, \mathbf{k} - \mathbf{q}_1 + \mathbf{q}_2) \right. \\ & \left. + (1 + N_{\mathbf{q}_1-\mathbf{q}_2}^{(\alpha)}) G(\omega - \sigma\omega_{\mathbf{k}-\mathbf{q}_1}^{(p)} - \omega_{\mathbf{q}_1-\mathbf{q}_2}^{(\alpha)}, \mathbf{q}_2) G(\omega - \omega_{\mathbf{q}_1-\mathbf{q}_2}^{(\alpha)}, \mathbf{k} - \mathbf{q}_1 + \mathbf{q}_2) \right] f^{(\alpha)}(\mathbf{k}, \mathbf{q}_1, \mathbf{q}_2) A_{\mathbf{k}-\mathbf{q}_1}^{(\sigma)}. \quad (10) \end{aligned}$$

The index  $\alpha = 1, 2$  is used in order to distinguish the two different self-energy diagrams depicted in Figs. 17,18. The two different cases of  $\alpha$  are obtained as follows:

- $\alpha=1$ . For the diagram depicted in Fig. 17 which involves only phonon loops  $\omega_k^{(\alpha)} = \omega_k^{(p)}$  where  $\omega_k^{(p)} = \Omega_0$  is the phonon frequency which we take it to be a constant characteristic optical phonon frequency  $\Omega_0$ . In this case  $f^{(\alpha)}(\mathbf{k}, \mathbf{q}_1, \mathbf{q}_2) = \gamma^4/N^2$ .
- $\alpha=2$ . For each of the diagrams depicted in Fig. 18 which involve one phonon and one spin-wave loop  $\omega_k^{(\alpha)} = \omega_k$  is the spin-wave excitation frequency and  $f^{(\alpha)}(\mathbf{k}, \mathbf{q}_1, \mathbf{q}_2) = \gamma^2/Ng(\mathbf{q}_1, \mathbf{q}_1 - \mathbf{q}_2)g(\mathbf{k}, \mathbf{q}_1 - \mathbf{q}_2)$ .

Here  $N_k^{(\alpha)} = 1/(e^{\beta\omega_k^\alpha} - 1)$ ,  $A_{\mathbf{k}}^+ = 1 + N_{\mathbf{k}}^{(1)}$  and  $A_{\mathbf{k}}^- = N_{\mathbf{k}}^{(1)}$ . The most significant vertex corrections due to purely spin-wave loops are given in Ref. 13 and are those of Fig. 19. Their contributions can be calculated at finite temperature in a simple way as follows. The contribution of the first two diagrams is obtained from the expression

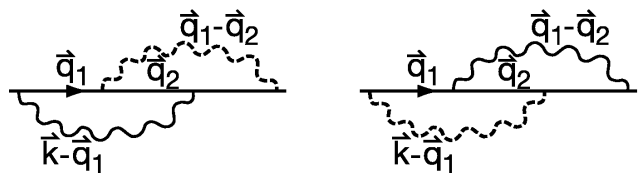


FIG. 18: The leading vertex corrections (two-loop) to the hole Green's function due to phonon (solid wiggly line) and spin-wave (dashed-wiggly line) loops.

given by Eq. 4 by multiplying it with the prefactor  $\zeta$  defined in Ref. 13 which is the factor that renormalizes the spin-wave velocity<sup>14</sup>. The contribution of the third diagram together with the leading order one loop diagram (given by Eq. 4) is obtained from the same expression given in Eq. 4 by replacing the spin-wave velocity  $\omega_k$  with  $(1 + \zeta)\omega_k$ . The last two-loop diagram of Fig. 19 is

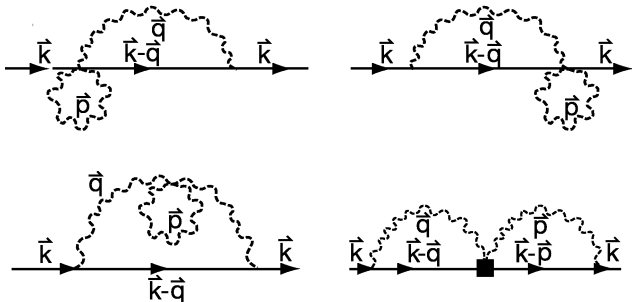


FIG. 19: The leading vertex corrections (two-loop) to the hole Green's function due to spin-wave loops.

given by the following expression:

$$\begin{aligned} \Sigma(\mathbf{k}, \omega) &= \sum_{\mathbf{p}, \mathbf{q}} \rho_2(\mathbf{q}, \mathbf{p}) F(\mathbf{k}, \mathbf{q}) F(\mathbf{k}, \mathbf{p}), \\ F(\mathbf{k}, \mathbf{q}) &\equiv g(\mathbf{k}, \mathbf{q}) \left( N_{\mathbf{q}}^{(2)} G(\omega + \omega_{\mathbf{q}}, \mathbf{k} - \mathbf{q}) \right. \\ &\quad \left. + (1 + N_{\mathbf{q}}^{(2)}) G(\omega - \omega_{\mathbf{q}}, \mathbf{k} - \mathbf{q}) \right), \end{aligned} \quad (11)$$

where  $\rho_2(\mathbf{k}, \mathbf{q})$  is defined in Ref. 13.

We found that the contribution from vertex corrections to be small even up to intermediate phonon coupling. However, the difference is significant in the strong coupling limit. Fig. 20 shows the spectral function with and without the vertex correction using  $\gamma = 0.2t$  (Fig. 20(a)) and  $0.5t$  (Fig. 20(b)) and  $\beta t = 10$ . As it can be inferred from Fig. 20(b) the lowest energy peak at  $(\frac{\pi}{2}, \frac{\pi}{2})$  becomes more broadened and there is more rapid transfer of spectral weight as we move along the  $(\frac{\pi}{2}, \frac{\pi}{2}) - (0, 0)$  direction. Hence, owing to the vertex corrections the “waterfall”-like feature, observed in the ARPES experiments, can be reproduced using smaller values of the electron-phonon coupling. If we include the vertex corrections the  $(\frac{\pi}{2}, \frac{\pi}{2})$  peak reduces its intensity and at strong enough coupling the  $(0, 0)$  high energy peak becomes more intense than the lowest energy peak. Therefore, we can remain in the intermediate coupling regime (e.g.,  $\gamma \sim 0.5t$  shown in Fig. 21) and still be able to reproduce a broadening similar to that observed in ARPES (bottom part of Fig. 21).

## VI. CONCLUSIONS

We have studied the  $t-J$ -Holstein model (including its  $t-t'-t''-J$  extension) at finite temperature within non-crossing approximation. We have also included vertex corrections due to the electron-phonon coupling. We find that the string excitations considered in Ref. 6 to account for the waterfall-like features of the spectral function observed in ARPES<sup>2,3</sup> are robust even at strong electron-phonon coupling and at room temperature. Furthermore,

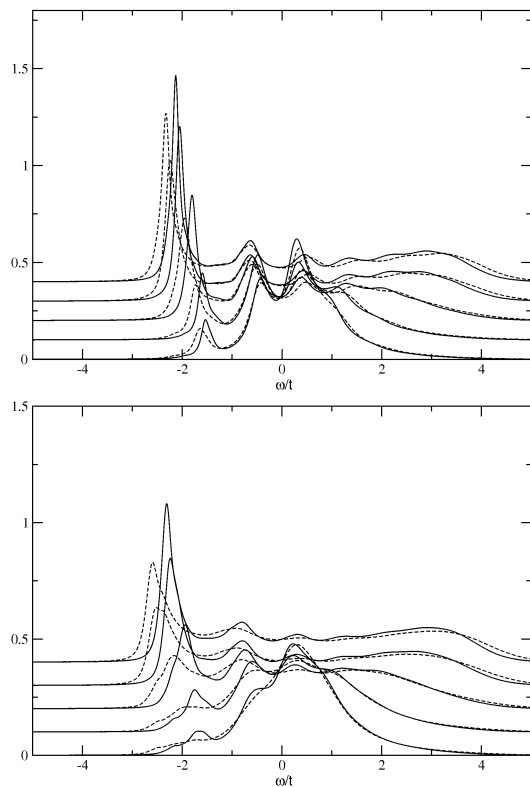


FIG. 20: Spectral function for (a)  $\gamma = 0.2t$  and (b)  $\gamma = 0.5t$  for  $\beta t = 10$  and on a  $16 \times 16$  lattice with (dashed lines) and without (solid lines) vertex corrections due to the electron-phonon interaction.

the hole spectral function obtained from the NCA treatment compares well with the reported ARPES intensity if we adopt a strong ( $\gamma/t \sim 1$ ) hole-phonon coupling. Namely, it exhibits the same general behavior found in Ref. 6, where an artificial spectral broadening was used in order to compare with the ARPES data; in the present treatment this agreement is achieved without using any such artificial broadening procedure. In the calculation reported in the present paper, the width and the energy dispersion of the lowest energy peak near  $(\pi/2, \pi/2)$  is reproduced and, in addition, we are able to qualitatively reproduce the high energy anomaly, i.e., the abrupt downturn in intensity which is characterised by two energy scales and the flat featureless intensity between them<sup>3</sup>.

Our calculation, where we included the leading-order vertex corrections due to the electron-phonon coupling, indicates that the vertex corrections are relatively small up to an intermediate coupling regime. We also found that in the strong coupling limit, they become significant, as expected. Furthermore, in order to reproduce the observed features in the ARPES spectra and intensity plots when we included the contribution of the vertex corrections, the value of the electron-phonon coupling needed to achieve the same qualitative agreement was found to be smaller than the one needed using our results obtained with the non-crossing approximation. This suggests that

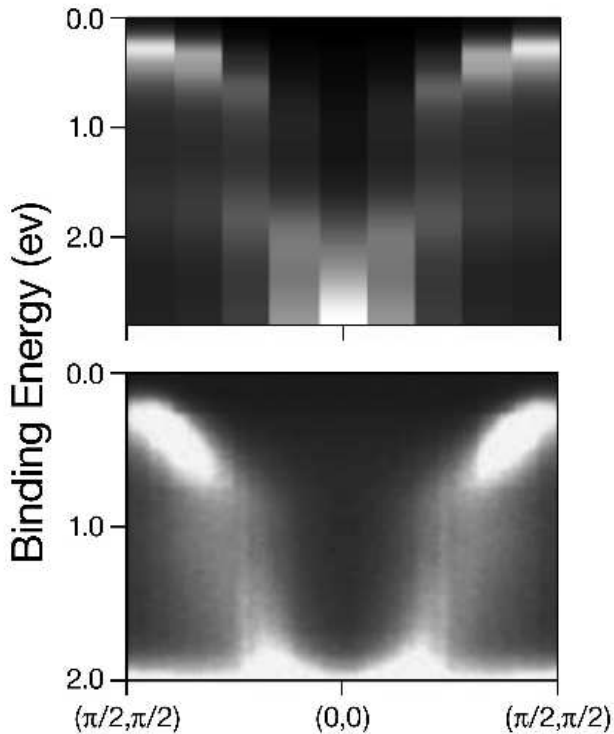


FIG. 21: Top: Calculated intensity plot of a  $16 \times 16$  lattice at  $\beta = 10$  for  $\gamma/t = 0.5$  where vertex corrections have been included. Bottom: ARPES intensity along the  $(0,0)$  to  $(\pi/2, \pi/2)$  direction.

the qualitative features of the results obtained within the non-crossing approximation (which is expected to fail in the strong coupling regime) might be valid in the regime describing the cuprate materials.

- 
- <sup>1</sup> A. Damascelli, Z. Hussain, Z.-X. Shen, *Rev. Mod. Phys.* **75**, 473 (2003).
  - <sup>2</sup> F. Ronning et al., *Phys. Rev. B* **71**, 094518 (2005).
  - <sup>3</sup> J. Graf et al., *Phys. Rev. Lett.* **98**, 067004 (2007).
  - <sup>4</sup> C. Kane, P.A. Lee and N. Read, *Phys. Rev. B*, **39**, 6880 (1989).
  - <sup>5</sup> Z. Liu, E. Manousakis, *Phys. Rev. B* **44**, 2414, *ibid* PRB**45**,2425 (1991). See also references therein.
  - <sup>6</sup> E. Manousakis, *Phys. Rev. B* **75**, 035106 (2007); E. Manousakis, *Phys. Lett. A* **362**, 86 (2007).
  - <sup>7</sup> P. Zhang, S. Louie, M. Cohen, *Phys. Rev. Lett.* **98**, 067005 (2007).
  - <sup>8</sup> P. Srivastava, S. Ghosh, A. Singh, *Phys. Rev. B* **76**, 184435 (2007).
  - <sup>9</sup> A. Macridin, M. Jarrell, T. Maier and D. J. Scalapino, *Phys. Rev. Lett.* **99**, 237001 (2007).
  - <sup>10</sup> M. M. Zempljic, P. Prelovsek and T. Tohyama, *Phys. Rev. Lett.* **100**, 036402 (2008).
  - <sup>11</sup> A. Lanzara et al., *Nature* (**412**), 510 (2001).
  - <sup>12</sup> C. Kim et al., *Phys. Rev. B* **65**,174516 (2002).
  - <sup>13</sup> Z. Liu, E. Manousakis, *Phys. Rev. B* **51**, 3156 (1995).
  - <sup>14</sup> E. Manousakis, *Rev. Mod. Phys.* **63**, 1 (1991).
  - <sup>15</sup> A. S. Mishchenko, N. Nagaosa, *Phys. Rev. Lett.* **93**, 036402 (2004).
  - <sup>16</sup> V. Cataudella et al., *Phys. Rev. Lett.* **99**, 226402 (2007).
  - <sup>17</sup> J. Jaklic, P. Prelovsek, *Phys. Rev. B* **55**, R7307 (1997).
  - <sup>18</sup> M. Brunner et al., *Phys. Rev. B* **62**, 15480 (2001).
  - <sup>19</sup> M. Berciu, *Phys. Rev. Lett.* **97**, 036402 (2006).
  - <sup>20</sup> G. D. Mahan, "Many Particle Physics" (Plenum Press, NY, 1990).
  - <sup>21</sup> A. A. Morales Jr., D. M. Yanga, S. Kurihara, *J. Supercond.* **15**(4), 277 (2002).
  - <sup>22</sup> T. Cuk et al., *Phys. Stat. Sol.(b)* **242**, No.1, 11 (2002).
  - <sup>23</sup> O. Gunnarsson and O. Rösch, *Phys. Rev. B* **73**, 174521 (2006).